Accepted Manuscript

Semi-interpenetrating network hyaluronic acid microgel delivery systems in micro-flow

Qiqing Chen, Andreas Passos, Stavroula Balabani, Alexandru Chivu, Shudong Zhao, Helena Azevedo, Peter Butler, Wenhui Song

Please cite this article as: Q. Chen, A. Passos, S. Balabani, A. Chivu, S. Zhao, H. Azevedo, P. Butler, W. Song, Semi-interpenetrating network hyaluronic acid microgel delivery systems in micro-flow, *Journal of Colloid and Interface Science* (2018), doi: https://doi.org/10.1016/j.jcis.2018.02.049

Semi-interpenetrating network hyaluronic acid microgel delivery systems in micro-flow

Qiqing Chen [a,b], Andreas Passos[c], Stavroula Balabani[c], Alexandru Chivu[b], Shudong Zhao[b], Helena Azevedo[d], Peter Butler[e], Wenhui Song[b]*,

[a] Plastic Surgery Department, Nanfang Hospital, Southern Medical University, Guangzhou, 510515, China;

[b] UCL Centre for Nanotechnology and Regenerative Medicine, Division of Surgery & Interventional Science, University College London, London, NW3 2PF, United Kingdom
E-mail: w.song@ucl.ac.uk;

[c] Department of Mechanical Engineering, University College London, London, NW1 2PS, United Kingdom

[d] School of Engineering and Materials Science, Queen Mary, University of London, Mile End Road, London, E1 4NS, UK.

[e] Department of Plastic and Reconstructive Surgery, Royal Free London NHS Foundation Trust, London, NW3 2PF, United Kingdom

E-mail: w.song@ucl.ac.uk

Abstract:

Macroscopic hydrogels are commonly used as injectable scaffolds or fillers, however they may easily obstruct blood vessels, which poses risks and limits their clinical use. In the present study, three types of hyaluronic acid (HA)-based hydrogel micro-particles with non-covalent, covalent semi-interpenetrating and conventional 3D molecular networks respectively, have been designed, fabricated and characterized. The micro-particles are spherical, biconcave or irregular in shape and their diameter ranged between 2.5 and 3.5 µm; their suspensions exhibit a tuneable viscosity, shear-thinning behaviour, dynamic stability and dispersity in microfluidic flow as a result of their specific particulate nature, providing thus a well-controlled injectable platform. Hydrogel particle suspensions also demonstrate an

1

enhanced safety profile, in terms of the dispersity, cell safety, and hemocompatibility. In addition, Rhodamine 6G has successfully been loaded and released from the particles as a model for drug delivery. Functionalisation of hydrogel microparticles using synthetic polymers has been proven to be a cost-effective way to achieve desirable rheological properties and flow dynamic stability with improved physicochemical properties and biocompatibility *in vitro*, showing promise as a multifunctional biomedical material for various advanced surgical devices and therapies.

1. Introduction

Macroscopic hydrogels are commonly used in the biomedical field, including scaffolds in tissue engineering,[1] vehicles for drugs or biomolecules,[2] and surgical materials.[3, 4] A common and attractive property of hydrogels lies in its injectability, which enables minimally invasive delivery. However, there is concern that hydrogels may block blood vessels, should the needle accidentally hit a vessel, as seen in soft tissue fillers or drug delivery systems. In some instances, such a blockage may result in serious complications, including massive tissue necrosis and blindness.[5] To make matters worse, there is no effective cure for such complications. Thus, much attention has been drawn to preventive measures, including anatomical education and introduction of blunt-tip cannulae.[6, 7] Unfortunately, these measures are not sufficient to eliminate such complications. Also, they are not suitable for every clinical situation.[8] Considering the high vascular density in certain tissue areas and the anatomical varieties, it is difficult to avoid at least some level of blood vessel damage during actual procedures.

One of the most important shortcomings many hydrogels share is their complex rheological behaviour, which varies as a function of the specific composition and the structure of the hydrogel network. With a yield stress and a shear-thinning property, many injectable

polymeric hydrogels may 'thin' quickly, i.e. may flow easier due to a decrease in viscosity with an increase of the pressure applied, compromising the controllability of delivery. If this happens in a blood vessel, a gel embolus may form immediately. Such emboli would not respond to thrombolytics. Furthermore, in the case of polymers with high molecular weights, a high viscosity can be reached at a low concentration and/or crosslinking degree. Thus, when the hydrogels are used as drug delivery systems, there is a trade-off between the injectability and the releasing kinetics, resulting in a compromised tunability.

As an important glycosaminoglycan existing in most of tissues of the human body, hyaluronic acid (HA) is widely used for tissue reconstruction and drug delivery due to its good biocompatibility and tuneable degradability. Meanwhile, synthetic polymers such as polyethylene glycol (PEG) and polyvinylpyrrolidone (PVP) are well known for their good hemocompatibility, molecular control and large-scale production. By combining the characteristics of natural and synthetic polymers, novel hybrid hydrogels can be developed, with improved physical/mechanical properties and biofunctions for various applications.[9-12] Since modification with hydrophilic molecules is a common method to further improve the hemocompatibility of biomaterials,[13] HA microgels functionalized with PEG or PVP, as a representative model of functionalized microgel system, may demonstrate both synergistic biocompatibility and hemocompatibility.[14] In comparison with the macroscopic and nanoscale counterparts, such a degradable microgel system is envisaged to improve cytological safety[15] and to cause less extensive ischemic damage with intravascular injection.[16] Meanwhile, it is expected to have good injectability and tunability, while maintaining good biocompatibility.

In the present study, physically and chemically modified HA microgels were designed, manufactured and characterized, with formation of PVP-HA and PEG-HA hybrid network, respectively. HA microgels with no modification were fabricated as the control. As

3

commercial HA dermal fillers are typical representatives of macroscopic HA-based hydrogels, a commercial HA filler sample was also used as an important reference in the rheological and swelling tests.

2. Material and methods

2.1 Materials

HA (average mw 500 kDa) was purchased from Bloomage Freda Biopharm Co., Ltd. PEG methyl ether (PEGME, mw 5 kDa), PVP (mw 10 kDa), Sorbitan monooleate (Span® 80), Rhodamine 6G, Hoechst 33258, 2-isopropanol, acetone, penicillin-streptomycin and light mineral oil were purchased from Sigma-Aldrich. Divinyl sulfone (DVS) was purchased from VWR. The Dulbecco's Modified Eagle Medium (high glucose, L-Glut, phenol red) and the foetal bovine serum were purchased from Life Technologies. The AlamarBlue reagent was purchased from invitrogen[TM]. Two millilitres of commercialized HA-based soft tissue fillers (BioHyalu, Freda Biopharm) was kindly provided by the Plastic Surgery Department, Nanfang Hospital, Guangzhou, China.

2.2 Preparation of mHA, mHA/PEG, and mHA/PVP

Hyaluronic acid was dissolved in deionised water to make the 10 mg/ml HA solution. PEGME and PVP were dissolved in deionised water to make 150 mg/ml solutions. DVS was dissolved in deionised water to make the 50 mg/ml solution.

Several drops of 2M NaOH were added to 3 ml of the 10 mg/ml HA solution to adjust the pH value in the range of 11 to 12. 100 μl of 150 mg/ml PEGME solution (PVP solution for mHA/PVP, deionized water for mHA, respectively) were added to the HA solution. Span® 80 was dissolved into mineral oil, with the volume ratio of 1 to 80. 12 ml of the resulting mineral oil solution were added to the previous HA/PEGME solution.

4

An ultrasonic processor (Model CP-750, Cole Parmer, USA) with a converter (Model CV-33) was used to prepare the w/o emulsion. During the ultrasonication, an amplification of 30% was selected, and the ultrasonication was run for three minutes. During the process, 0.6 ml of 50mg/ml DVS solution was added. The reaction was allowed to proceed for one hour at room temperature without intervention.

Next, the oil phase was washed away with 16 ml isopropanol for mHA/PEG and mHA, and 16 ml acetone for mHA/PVP. Following agitation, the mixtures were centrifuged at 3000 rpm for 15 minutes. The precipitate was collected and washed several more times. The precipitate was dried under a negative pressure and re-suspended in deionised water.

2.3 Characterization

2.3.1 Fourier transform infrared spectroscopy

All FTIR measurements were carried out with Jasco FT/IR-4200 (Jasco Co. Ltd., Japan). Absorbance spectra were recorded for uncrosslinked HA, mHA/PVP, mHA/PEG, and mHA. In order to fit the baseline and to minimise the effects of the slopes on absorbance peaks, Essential FTIR^{TM} v.3.50 was used to analyse the raw data and generate second derivative spectra, with the Savitsky-Golay algorithm as the smoothing method. The derivative spectra were further manipulated with vector normalization to correct the scattering effect and to normalize the baseline. The intensity of N-H bending peak was measured. The N-H bending intensities in mHA/PVP, mHA/PEG and mHA were compared to that of uncrosslinked HA, to determine the relative content of HA in the products.

5

2.3.2 Dynamic light scattering assay

In order to determine the average size of the particle units, including individual hydrogel particles and particle clumps in the suspension, dynamic light scattering (DLS) measurements and analysis were performed with a DelsaMax Pro analyser (Beckman Coulter, Inc, USA). For each suspension, a concentration of 2 mg/ml (0.2 wt %) was used to run the assay. The measurements were carried out at 25 °C. The average sizes, and size distribution (the PDI) of the peaks were recorded.

2.3.3 Particle morphology

The particle sizes were confirmed with a scanning electronic microscope (SEM, LEO 1540XB, Zeiss, Germany). To prepare the SEM samples, diluted suspensions were dropped on adhesive carbon tabs, placed on SEM stubs, and lyophilized overnight. After the freeze-dry procedure, the samples were coated with gold and stored in a vacuum desiccator prior to the analysis.

2.3.4 Rheological characterisation

A rheometer (Malvern) was employed to assess the rheological behaviour of suspensions of mHA/PVP, mHA/PEG, mHA, as well as the commercial filler. The concentration of the commercial filler sample was measured to be 50 mg/ml (i.e. 4.8 wt% or 2.8 vol%, HA density= 1.8 g/cm^3).by weight measurement after freeze-drying. Samples used in rheological assessment shared the same concentration as the commercial filler.

A steady shear test was performed and flow curves of shear stress and effective viscosity versus shear rate respectively were generated for each sample. A frequency sweep was also applied to every sample, in order to characterise the dynamic viscoelasticity of the three suspensions at a low strain amplitude (0.5%). The stress-strain relationship of all three suspensions was also analysed with the Herschel-Bulkley model[17]:

6

$$\tau=\tau_y+K\gamma^n$$

where τ_y is the yield stress, K the consistency and n the flow index. The parameters of the model fitted to the acquired data were calculated and listed in Table 1.

2.3.5 Microfluidic experiments with hydrogel particle suspension flows

In order to understand the behaviour of the particles in the blood stream, microfluidic experiments were conducted to preliminarily study the flow field of the suspensions upon entering a continuous flow stream.

Microfluidic system set up

A pressure controlled perfusion system described elsewhere[18] was used to deliver the suspension flows through the side branch of a rectangular T-junction microfluidic device comprising a 500μm wide microchannel with a 100 μm wide branch. The height of the channels was 100 μm resulting in an aspect ratio of 5:1 in the main channels and 1:1 in the side branch. The microchannel was made of polydimethylsiloxane (PDMS) and fabricated using standard soft lithography techniques. [19]

The microfluidic channel was placed on an inverted microscope (DMILM: Leica, Germany) with a 10x objective. The flow was illuminated by a green LED microstrobe and a Hamamatsu C8484-05C CCD camera (Hamamatsu, Japan) was used for imaging. A 35 vol% glycerol in aqueous solution was perfused into the 500 μm main channel, with a flow rate of 100 μL/min, using a syringe pump. Particle suspensions (20 mg/ml) were injected through the 100 μm branch in a continuous manner, using the pressure control system [18]. An external injection pressure of 28kPa was applied to the syringe to simulate the injection process and to generate shear conditions in the physiological flow range for the microcirculation.

7

Characterisation of Hydrogel Particle Micro-Flow Dynamics

60 successive image pairs of the microgel flows were acquired at a time interval of 0.5 ms upon entering the microfluidic T-junction and 1 cm (20 channel widths) further downstream in order to compare the ensuing flow patterns for the different samples and to observe any potential particle aggregation. Using the hydrogel particles as tracers, multipass cross-correlation, micro-particle image velocimetry (μPIV) algorithms were implemented in JPIV v13.08 (www.jpiv.vennemann-online.de) in order to determine the velocity field. The inlet flow velocities of the microgel suspensions were estimated from the PIV data. These were: 60 mm/s for mHA/PVP, 19 mm/s for mHA/PEG and 52 mm/s for the mHA. The continuous phase flow velocity was kept constant at 33.3 mm/s and the corresponding dispersed to continuous phase velocity ratios (u_d/u_c) were 1.8, 0.6 and 1.6 respectively. The viscosity ratios (μ_d/μ_c) were 0.17, 0.6 and 0.4 for the mHA/PVP, mHA/PEG and mHA respectively.

2.3.6 Swelling ability

The dried precipitate was dipped into deionized water for one hour. The supernatant was removed, and the surface of the precipitate was dried by a piece of absorbable tissue. The wet precipitate was weighed. The wet precipitate was then dried again and weighed.

The mass swelling ratio (MSR) was calculated as follows:

$$MSR = \frac{Hydrated\ weight - Dehydrated\ weight}{Dehydrated\ weight}$$

2.3.7 In vitro enzymatic degradation assessment

Excessive particle aggregations were added into 2 ml of hyaluronidase solution (0.5 mg/ml). The mixture was placed in a centrifuge tube, and was incubated at 37 °C for 1.5 hours and 3 hours, respectively. Then, the supernatant was collected. In order to ensure complete degradation, the collected liquid was placed at room temperature for 120 hours before

8

colorimetry was carried out with Ehrlich's reaction. The absorbance at 562 nm was measured with a plate reader (BioTek Instruments, USA), and the molar concentration of N-acetyl-D-glucosamine was calculated with a standard curve. Three batches of samples were measured.

2.3.8 Effects on thrombosis

Thromboelastography (TEG 5000, Thrombelastograph® Analyzer, Haemoscope, USA) was employed to assess the effect of hydrogel particles on thrombosis. Citrated whole blood was tested (HTA Licence: 11016; project code: NC2016.006). A total volume of 360 µl was used in the test. Twenty microliters of calcium chloride ($CaCl_2$) were added with 36 µl suspension (25 mg/ml) into 304 µl fresh citrated whole blood. To mimic the diluting effect of adding suspensions, a PBS control was used to dilute blood to the same extent. The test was run as long as stable values were obtained. The values of angle α and maximum amplitude (MA) were selected to compare the effect of suspensions on thrombosis.

2.3.9 Effects on cell metabolism and viability

Human dermal fibroblasts (HDFs, passage 15) were used to test the subacute toxic effects of hydrogel particles. The test included two different final concentrations of each suspension, i.e. 1 mg/ml and 2 mg/ml. PBS control groups were used. HDFs were cultured in 48-well plates, 6200 cells each well, with 500 µl culture medium each well, and incubated at 37°C. Single doses were given to all the cell cultures. The dosages were delivered 24 hours after seeding the cells, when anchorage was confirmed with an optical microscope. The alamarBlue assay was used to evaluate the effect on metabolism, and the total DNA quantification was used to assess the effect on viability. After receiving single doses, the cells were tested on day 6.

In the alamarBlue test, a positive control was prepared by autoclaving the reagent-media mixture for one cycle. A no-cell control was prepared by incubating the mixture at 37℃. A fluorescence plate reader (Fluoroskan Ascent FL, Thermo Labsystems) was used to assess the

reduction rate of the dye, with a pair of filters for excitation 570 nm and emission 620 nm. The reduction rate was calculated as follows:

$$Reduction\ rate = \frac{Sample\ reading - No\_cell\ control}{Positive\ control - No\_cell\ control}$$

A commercial quantification kit was used for total DNA quantification. The same fluorescence plate reader was used, with a pair of filters for excitation at 355 nm and emission at 460 nm.

2.3.10 Preliminary loading and release test

In order to incorporate Rhodamine 6G into the hydrogel particles, a 20 µl 5mg/ml Rhodamine 6G solution was added into the water phase before ultrasonication. The hydrogel particles were manufactured following the process described previously.

The *in vitro* releasing test was carried out with washed precipitate loaded with Rhodamine 6G, under the enzymatic catalysis with bovine hyaluronidase. A fluorescence microscope (Nikon ECLIPSE Ni) was employed to assess the loading status of Rhodamine 6G, using excitation at 532 nm. A UV-VIS spectrometer was used to measure the absorbance at 539 nm. The dried precipitate was cut to fit the bottom of 1.5 ml UV cuvettes and placed in such a way that the light pathway remained unobstructed. 1ml of deionised water and 0.5ml 1mg/ml hyaluronidase was added into the cuvettes, immediately followed by the measurement of time point 0. The measurement was carried out every 20 minutes, for 3 hours.

2.3.11 Statistical analysis

The IBM SPSS v23.0 software package was used to carry out the statistical analysis in the present study. The average values were compared with One-way ANOVA when homogeneity of variance was accepted. Otherwise, the non-parameter test of Kruskal-Wallis analysis was used.

10

3. Results and discussion

3.1 Synthesis of hydrogel micro-particles

In the present study, an ultrasonic invert emulsion was used to manufacture the hydrogel particles. Compared to the invert emulsions generated by vigorous stirring,[20] ultrasonication improved the efficiency of particle production, reduction and uniformity of particle size resulting in more stable emulsions.[21] This is especially important for HA molecules in the precursor solution, as the intermolecular entanglement may decrease the efficiency.[22]
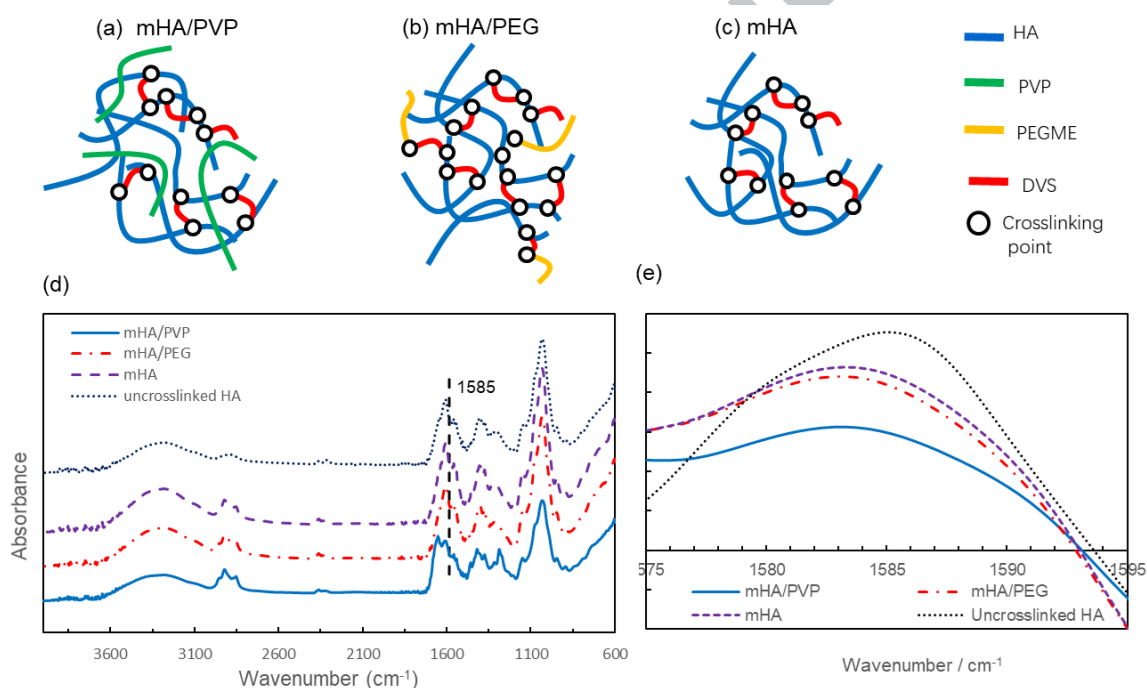

Figure 1. (a)-(c) Schematic showing semi-interpenetrating network of HA/PVP (a). interpenetrating network of HA/PEG (b) and network of HA(c). (d) FTIR spectra of the three hydrogel microparticles. (e) Vector normalized second order derivative FTIR spectra between 1575 and 1595 cm^{-1}, generated with the Savitsky-Golay algorithm, which narrowed the bandwidths and increased the resolution of differential spectra. In uncrosslinked hyaluronic acid, the peak around 1585 cm-1 represented N-H bending, which was used as a marker of HA molecules.

As one of the most commonly used crosslinkers in the industry of HA-based fillers,[23] divinyl sulfone (DVS) was selected. The crosslinking reaction could take place at room temperature.[24] The reaction rate was high with most crosslinking completed within the first 30 minutes,[25] which is also important in terms of manufacturing efficiency. As for the final products, different crosslinking degrees can be achieved by altering the ratio of HA and DVS.[26] A mass ratio of 1:1 was used in the present study. This mass ratio was shown to result in a crosslinking degree as high as 90%.[26] Three types of hydrogel micro-particles with different polymeric networks were produced: non-covalent semi-interpenetrating mHA/PVP network, covalently bonded semi-penetrating mHA/PEG network and conventional mHA network, as illustrated in Fig. 1a-c.

3.2 Size and morphology of hydrogel microparticles

The average size of the fabricated hydrogel particle units was measured by dynamic light scattering. A dilute suspension of particles, 2 mg/mL (~0.2 wt %) was employed in the DLS tests in order to minimise the potential aggregation and ensure that the particles were well dispersed. The results are summarized in Table 1. The average diameter of the polymer modified particles recorded from three repeated measurements was approximately 3.4 μm, with the smaller size of mHA, around 2.5 μm. Being smaller than red blood cells (about 8 μm),[27] the hydrogel particles should be able to flow through the capillary network without causing significant occlusion. Kruskal-Wallis analysis showed that the mean diameter of the particle units in mHA/PVP (3.39 ± 0.65 μm, mean rank = 9.4) was similar to that of mHA/PEG (3.44 ± 0.09 μm, mean rank = 11) ($p > 0.99$), while that of mHA (2.59 ± 0.42 μm, mean rank = 3.6) was significantly smaller ($p < 0.04$). The particles exhibited a low polydispersity index (PDI) in all suspensions characterised, and hence the particle size distributions can be considered near monodisperse (Table 1). However it should be noted that the refractive index =1.333 for solid HA was only available and employed for DLS analyses

12

for all three particles based on an ideal sphere model. The effects of the unknown refractive index of the hydrogels and non-spherical geometries of the particles (Fig. 2) on the measurements of the particles size and PDI require further investigation.

Table 1. Summary of structure and properties of the peaks detected in hydrogel particle suspensions

	mHA/PVP	mHA/PEG	mHA
DLS No. of peak	1	1	1
Mean particle diameter,(μm)	3.39 ± 0.65	3.44 ± 0.09	2.59 ± 0.42
Polydispersity index, PDI	0.07 ± 0.03	0.08 ± 0.03	0.15± 0.02
Relative HA content%	56.9 ± 8.01	80.1 ± 2.04	84.5 ± 6.60
Mass swelling ratio, MSR	7.01 ± 3.95	7.93 ± 3.39	10.40 ± 5.68

The relative content of HA in the three particle types was quantified by FTIR (Fig 1d). Because the N-H bond is only present in HA and it remained unreacted throughout the manipulation, the relative intensity ratio of the N-H bending peaks was used to determine the relative content of HA in the three samples. The FTIR spectra were transformed to second derivative spectra, as shown in enlarged spectra between 1500 and 1600 cm^{-1}, i.e. the amide II region, before vector normalization was applied to minimise the effects of scattering (Fig. 1e). A slight red shift was observed after the crosslinking, indicating that the reduction of the number of hydroxyl groups had an effect on hydrogen bonding. Despite of the red shift, all the corresponding peaks for the three particles were located between 1500 and 1600 cm^{-1}.[28] The intensity of the peak is proportional to the molar content of the repeating units of HA molecules. The intensity of the peaks was 0.055, 0.046, 0.044 and 0.031, in uncrosslinked hyaluronic acid, mHA, mHA/PEG, and mHA/PVP, respectively. Based on these results, the relative contents of HA in mHA, mHA/PEG, and mHA/PVP, were computed to be 84.5%,

13

80.1%, and 56.9%, respectively. One-way ANOVA showed that the ratio was significantly lower in mHA/PVP, compared to that of mHA/PEG (p = 0.004) and mHA (p = 0.01).

The HA content measured in the hydrogel particles may reflect different hydrogen bonding interactions between polymer molecules. Compared to the oxygen in the ether bond (-O-) of PEGME backbone, the oxygen on carbonyl double bond (>C=O) in cyclic amide side group of PVP is more electronegative[29, 30] and attractive to hydrogens bearing a partial positive charge. Therefore, a stronger hydrogen bonding network may form between PVP and HA chains, resulting in an increased amount of PVP incorporated. On the other hand, although PEGME may form covalent connections with HA, only one hydroxyl end group exists per molecule. Apparently, this was not sufficient to offset the effect of hydrogen bonds. Previous studies also showed that PVP can form a more stable network compared to PEG; as a result, the interaction energies and the electron density may be affected.[31] Both carbonyl bond (>C=O) and cyclic amide (>N-) of PVP side groups can contribute to the hydrogen bond with hydrogen from glycerol and water molecules.
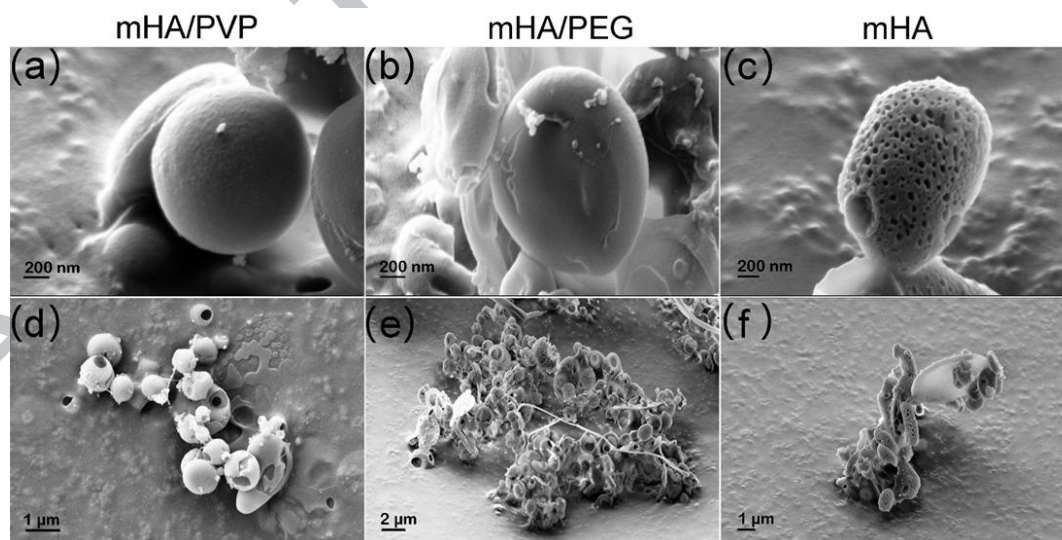

Figure 2. SEM images showing the morphology of microparticles made from mHA/PVP (a) and (d), mHA/PEG (b) and (e) and mHA (c) and (f).

The particle morphology was assessed with SEM (Fig. 2). Most imaged particles exhibited a diameter between 1.5 and 3 µm, slightly smaller and less uniform than the DLS measurement results indicated in Table 1. Discrepancy of the particle measurements by different characterisation equipment is an existing issue due to the different principles and assumptions on which each technique is based. In the case of the SEM measurement, a small shrinkage of the hydrogel particles, caused by a freeze-dry process in the sample preparation, may be argued to be one of reasons that smaller particles were seen. Nevertheless, the morphology of the freeze-dried hydrogel particles provide more information about the shape and surface structure of the networks. In mHA/PVP (Fig. 2a) and mHA/PEG (Fig. 2b), spherical and oval particles with smooth surfaces were observed. Some of the mHA/PVP particles have a hollow core, like pitted olives (Fig. 2d), while most mHA/PEG particles show more dumbbell-like shape, reminiscent of biconcave red blood cells (Fig. 2e). However, mHA particles exhibited a porous surface with an increased irregularity, both in shape and size (Fig. 2c and 2f). The different morphologies may be attributed to different 3D network structures in each particle as illustrated in Fig. 1a-1c. The smooth and condensed hydrogel particles indicate that a uniform 3D network formed because of either non-covalent or covalent semi-interpenetration of PVP and PEG chains throughout the HA network. In the case of HA hydrogel alone, the porous morphology of mHA particles may indicate that a non-uniform local crosslinking reaction occurred with DVS resulting in a phase separation within the 3D network between densely crosslinked HA rich domains and water rich domains. This may be attributed to the non-uniform distribution of DVS among the HA network with highly entangled molecular chains owning to the high molecular weight.

In principle, the synthesised particles should be able to circulate through most of the capillary network of the human body in terms of their size (mean diameter 3 to 4 µm).[32] The possibility of blood vessel occlusion is small based on the result given by DLS, but a small

number of local infarctions caused by larger particle aggregates/clumps are still possible. This indicates that the clinical safety profile of the synthesised particles is remarkably improved compared to macroscopic hydrogels. Macroscopic hydrogels can block larger vessels with a relatively small volume, affecting all downstream branches and resulting in massive ischemia. Commercially available HA dermal fillers for example, may cause irreversible blindness, due to blockage of the central retinal artery if injected into the supratrochlear artery.[33] Given the same injecting volume, the blockage caused by particle clumps, if any, would be limited due to their potential dispersity and disaggregation at high shear rate. The collateral circulation and the compensatory mechanism would further reduce the infarction area. However, scattered infarctions of retinal capillaries, as seen in diabetic retinopathy, do not necessarily cause blindness.[34]
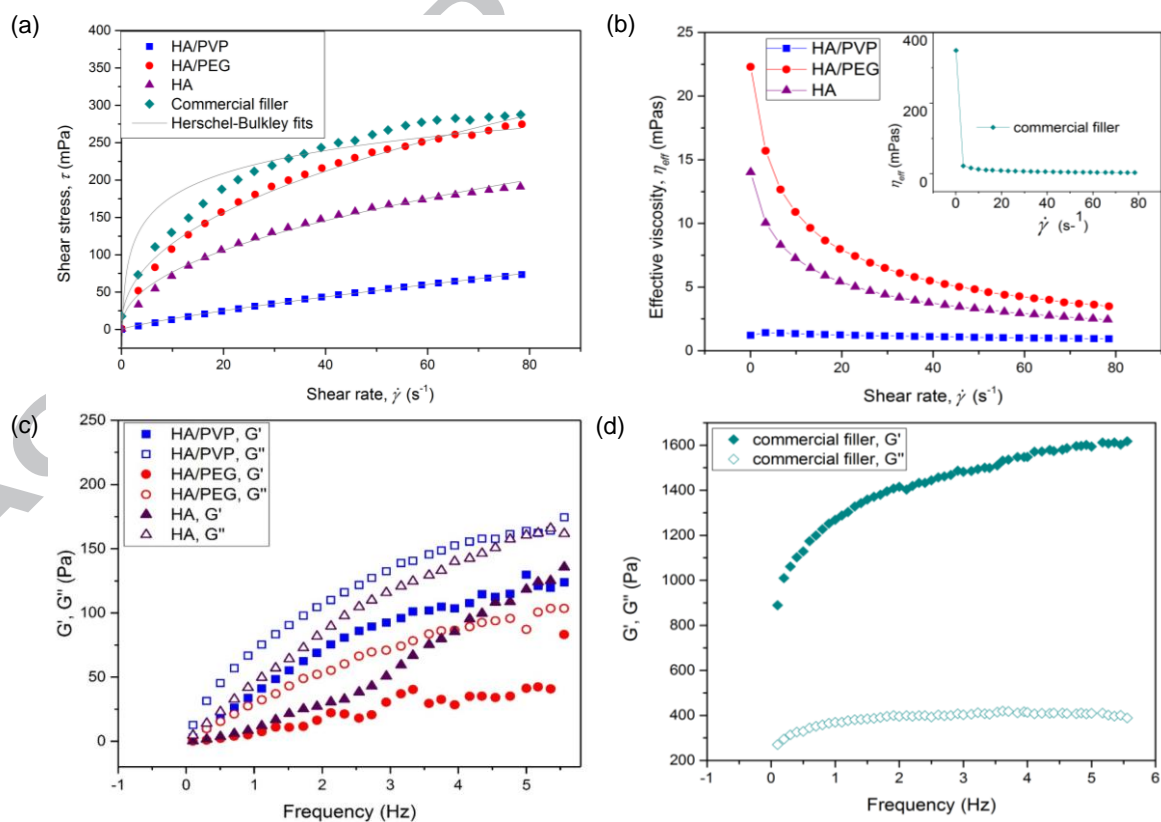
3.3 Rheological properties

Figure 3. (a) Shear stress versus shear rate curves of particle suspensions and the commercial filler, and fitting with the Herschel-Bulkley model. (b) Effective viscosity versus shear rates curves of particle suspensions and the commercial filler. (c) Frequency dependence of storage modulus G' and lost modules G'' of the three suspensions. (d) Frequency dependence of storage modulus G' and lost modules G'' of the commercial filler.

For comparison purposes, all samples rheologically characterised shared the same concentration with that of the commercial fillers (50 mg/ml). The effective viscosity was measured at 25°C using steady shear measurements. The variation of the shear stress and viscosity with shear rates are shown in Fig. 3a and 3b, respectively. The shear stress-shear rate data were fitted with the three parameters of Herschel-Bulkley model[17] to provide additional insight into the rheology of the particle suspensions. The corresponding model parameters are given in Table 2. All samples demonstrated negligible yield stress and shear-thinning (pseudoplastic) behaviour as indicated by their flow index n<1; mHA/PVP showed a more Newtonian like behaviour with its flow index approaching n=0.8. Notably, the viscosity of the commercial filler at zero shear is an order of magnitude higher than that of the fabricated hydrogel particles, which can be attributed to its continuous 3D molecular network structure (Fig. 3b), and drops sharply in the low-shear-rate region, in contrast to the gradual thinning behaviour observed in the present particle suspensions. Although the Herschel Bulkley model could not be fitted to the commercial filler data, extrapolation of the shear stress-shear rate data to zero shear indicates that the filler exhibits a relatively high yield stress (Fig. 3) and 'thins' rapidly when the shear rate increases. This explains the difficulties associated with injecting soft tissue fillers initially, and the sudden bursting out of the needle when the pressure applied exceeds a certain level - that of the filler yield stress. Should this happen in a blood vessel during injection, devastating complications would follow.

17

Table 2. Rheological parameters of three hydrogel particle suspensions from Herschel-Bulkley model.

	HA/PVP	HA	HA/PEG
Yield stress, τ_y	0	0	0
$\sigma(\tau_y)$	0.58	5.82	9.32
Consistency, K	2.31	26.66	41.93
$\sigma(K)$	0.16	3.71	6.28
Flow index, n	0.80	0.46	0.44
$\sigma(n)$	0.01	0.03	0.03

Compared to the commercial filler, the particle suspensions showed negligible yield stress and a gentler drop in viscosity in the low-shear-rate region, endowing the suspensions with better control during the injection process. It can be seen form Figure 3 and Table 1 that the three suspensions exhibit different shear thinning behaviour with the suspension of mHA/PVP particles exhibiting the lowest viscosity (2.39 mPas) at the low shear region. This indicates that mHA/PVP can be easily injected with finer needles, causing less pain, [35] and reducing local inflammatory responses. It is also suitable for precise treatment of tiny depressions. It is worth noting that PVP is used as lubricant in some eye drops. Particle morphology can partly explain the differences in the shear thinning behaviour of the three suspensions. For example, mHA/PVP particles are smooth and spherical (Fig. 2a) possibly due to a large number of hydrophilic pyrrolidone side groups on PVP chains that enhance the affinity between HA and PVP within the particles. Thus a rheological behaviour typical of hard spheres well studied in the literature should be expected; mHA/PEG and mHA particles on the other exhibit non-spherical morphologies that are known to increase viscosity. mHA/PEG particles are shown to have a discoid shape and mHA an irregular oval shape which result in additional energy dissipation due to particle-particle interaction and particle orientation in flow. The porosity and surface roughness of the three particles as well as their Young modulus may also play a role. It should be noted that although the mass concentration of the three particles was kept

18

the same as the commercial HA filler, the volume fraction of the three suspensions might be slightly different and hence caution should be exercised when directly comparing the flow curves of the three suspensions.

Dynamic rheological characterisation using frequency sweeps at a low strain amplitude (0.5%), showed that all three hydrogels exhibited time dependent viscoelasticity with an increase of the storage (G') and loss moduli (G'') with increasing oscillatory frequency (Fig. 3c and 3d). For all three suspensions, the values of G'' were always larger than G', indicating that viscous behaviour is predominant in the three suspensions due to the weak physical network among the hydrogel micro-particles. Nevertheless, mHA/PVP possesses the highest storage modulus and mHA/PEG the lowest among the three suspensions. This indicates a stiffening effect by PVP and softening by PEG In contrast, the G' of the bulk gel (the commercial filler) was markedly higher than G'', indicating dominance of elastic behaviour at small strains and stiffening at high frequency owing to its continuous network through both covalent and non-covalent bonding of HA chains.

3.4 Microscale suspension flow dynamics

A T-junction microfluidic system (Fig. 4a) was employed to evaluate the dispersity and flow dynamics of the hydrogel particle suspensions at the microscale, mimicking the injection condition process in surgical practice. A 500μm main channel with a 100 μm side branch was designed and fabricated in order to mimic the injection process through a 32-gauge needle, with an internal diameter of 97 μm, into a small vessel. A blood analog solution of 35% glycerol/65% water was perfused through the main channel at a constant flow rate of 100 μl/min resulting in shear rates considered to be physiological at the level of the microcirculation.[36] The viscosity of the 35% glycerol solution was measured at 5.80 mPas, which is close to the viscosity of healthy whole blood [37]. As shown in Fig. 4b-j, all

19

suspensions were observed to flow into the main channel, without forming aggregates sticking to the side wall due to the high shear stress.
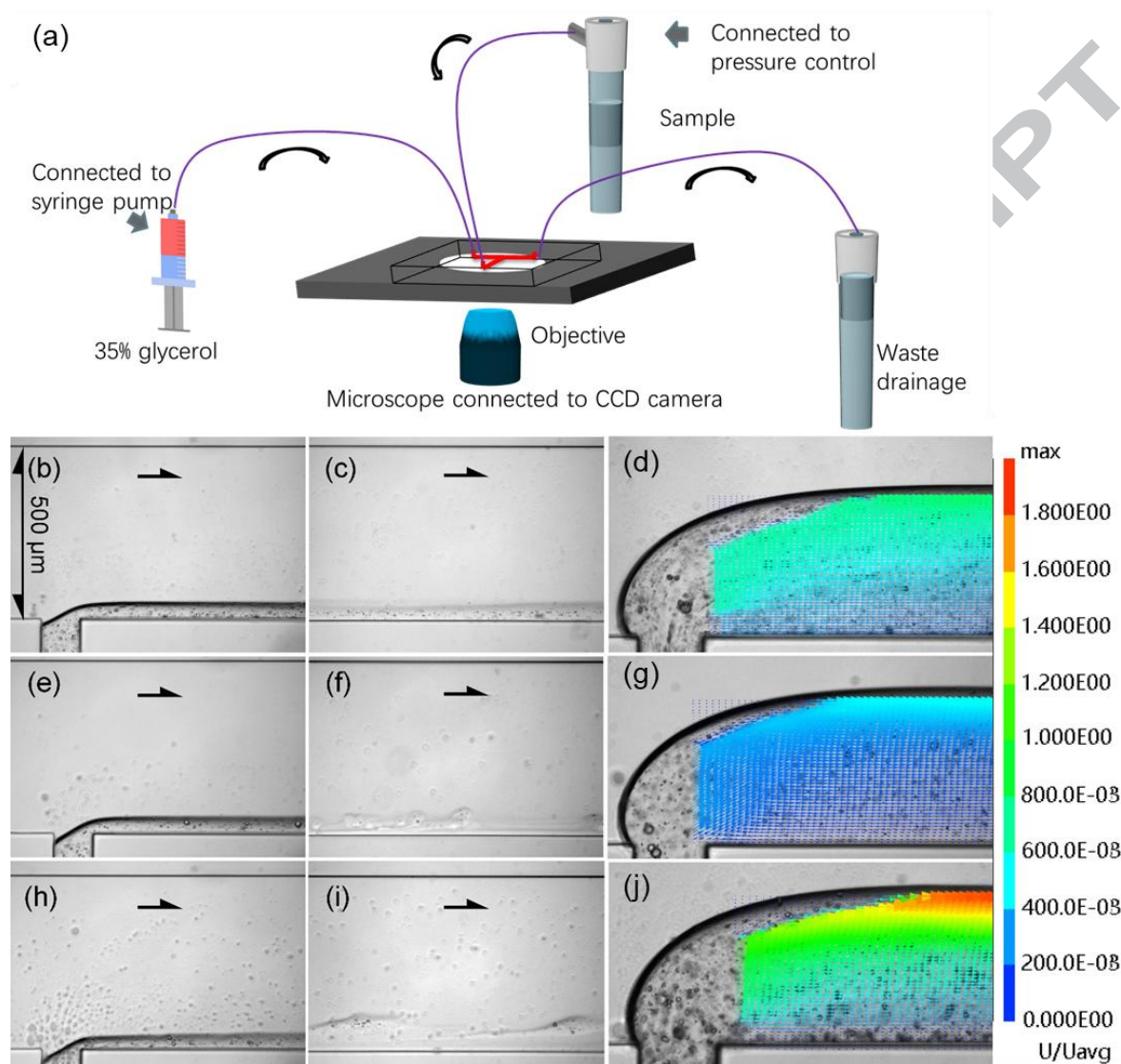

Figure 4. a) Schematic of A T-junction microfluidic system. (b-j) The flow fields of three particle suspensions at the T-injection port (b, e, h) and the site 1 cm away (c, f, i). As the arrow indicates, a 35% glycerol solution was fed into the main channel using a syringe pump. (d), (g) and (j) show the velocity distribution of three particle suspensions (external injection pressure = 28 kPa). The velocity vectors are normalised with the average velocity across the microfluidic channel obtained from the combined flowrate of the two streams in order to facilitate comparisons. The red indicates high velocity, while blue low velocity. (b, c, d) mHA/PVP; (e, f, g) mHA/PEG; (h, i, j) mHA.

The particle suspension flows (dispersed phase) enter the main channel with velocities ranging from around 20 to 60 mm/s depending on the type of hydrogel suspension delivered under controlled constant pressure. Upon encountering the continuous phase flow, a parallel (co-flow) flow pattern emerges characterised by the presence of a liquid-liquid interface separating a thin layer of the dispersed particle suspension and the continuous flow phase which move parallel to each other (Fig. 4b, 4e and 4h). As the main channel is 5 times wider than the side one the flow is fairly unconfined which, combined with the flow conditions of the experiment, result in the dispersed flow jet unable to penetrate deep into the main flow but rather to remain narrow and parallel to the channel wall. The continuous flow velocity is comparable or lower to that of the dispersed phase (33 mm/s) and hence the shear forces are not sufficiently high to destabilise the interface of the incoming dispersed jet flow; hence the flow pattern appears fairly stable for a few channel widths downstream of the junction (Fig. 4b, e, h). The two phases are both aqueous and hence partially miscible and particles manage to cross the interface and disperse into the water-glycerol solution because of their hydrophilic nature. Furthermore, the low interfacial tension between the two phases is expected to promote the formation of long threads or jets of the dispersed phase as suggested by literature[38] and these might be difficult to destabilise. Nevertheless, images obtained 20 channel widths downstream of the T-junction (Fig. 4c, 4f and 4i) show that this is not the case. The three types of hydrogel micro-particles exhibit distinctly different flow behaviour. Only the mHA/PVP particle suspension seems to remain flowing continuously near the channel wall with a gradually expanded particle suspension zone and a fairly stable liquid-liquid interface present. In contrast, both mHA/PEG and mHA dispersed phases appear to have lost their dynamic stability, as evidenced by the discontinuous or wavy interface seen in Fig 4f and 4i. This can be attributed to the different flow and viscosity ratios between the continuous and dispersed phases among the three hydrogel suspension systems as well as their corresponding viscoelasticity. Although the three suspension systems were 'injected' by

21

applying the same pressure differences in viscosity result in the dispersed phase to continuous phase velocity ratio to differ in the three systems. The average inlet velocity of the mHA/PVP suspension was estimated to be almost twice that of the continuous phase (and its viscosity the lowest) which implies a high jet velocity suppressing or converting away any flow perturbations and hence promoting the formation of a continuous dispersed flow stream near the wall. This can be seen in Fig. 4d in which the vector field of the mHA/PVP dispersed flow, obtained through quantitative imaging techniques, is superimposed on the acquired images. The high velocities of the incoming dispersed flow jet are evident. On the contrary, mHA/PEG and mHA are more viscous than the HA/PVP and hence enter the T-junction with slightly lower velocities. As a result the velocity ratio between the dispersed and continuous phase is lower (20 and 50 mm/s) and the viscosity ratio higher compared to that in the mHA/PVP case, which destabilises the dispersed phase stream. The vector plots in Fig. 4g and 4j illustrate the different flow behaviour of the mHA/PEG and mHA suspensions characterised by lower flow velocities in comparison to the mHA/PVP case and high velocities been confined in a small region near the interface.

It should be noted that unlike reported liquid-liquid flows in T-microchannels, the dispersed flows in the present study comprise particle suspensions. Particle suspensions are known to exhibit shear induced migration at low shear flows; this migration depends on particle properties as well as the viscoelasticity of the matrix and may further contribute to the flow dynamics of the suspensions under study. The surface chemistry, and morphologies of the three types of particles differ markedly despite sharing the same concentration (wt %) in their suspension. It can be argued that the microflow behaviour of the mHA/PVP particle suspension can also be attributed to reduced migration, compared to anisotropic discoid shaped mHA/PEG and irregular porous mHA particles that are expected to exhibit potential tumbling and rotation in shear and hence enhanced migration away from the wall.

22

Furthermore, blood itself is a soft particle suspension and its behaviour cannot be accurately replicated by blood analogs such as the one employed in the present study. Red blood cells may interact with the hydrogel particles resulting in non-uniform particle distributions across the channel and hence a local viscosity variation. For example, red blood cells are known to cause margination of drug delivery particles.[39] Such effects depend on particle characteristics and merit further investigation, which is beyond the scope of this study.

Finally, according to aggregation theory, low shear conditions can cause clustering of neighbouring particles, and thus formation of aggregates.[40]. Shear induced aggregation is a well documented phenomenon of particle suspensions and is reversible, i.e. aggregates break down as shear is increased. In the context of the present study, such aggregate formations can potentially block the channel and form gel emboli. The flow rates employed in the present study (100 μL/min) result in nominal shear rates of around 300 s^{-1}; these are physiological for microvascular flows and relatively high for aggregate formation; however, a shear rate distribution is expected in the microchannel which might favour local aggregate formation.[41] No such aggregate formation was observed for the three hydrogel particle systems under the low flow conditions studied and hence it is unlikely that the channel would be occluded with higher flow velocities.

3.5 Swelling ability

The mass swelling ratio (MSR) has been used to quantify the water absorption of HA.[42, 43] Since the MSR is inversely related to the crosslinking degree, hydrogels with a high MSR may also have a limited longevity in the human body, due to the low crosslinking degree and thus the reduced resistance to hyaluronidases.

Although no significant difference was found among the three hydrogel particles, all the particles had a lower MSR (mHA/PVP 7.01, mHA/PEG 7.93, mHA 10.40) compared to the

23

commercial filler sample (23.63, p < 0.005) (Table 1). This indicated that the particles had a higher crosslinking degree. Potential experimental errors of under-measurement of the MSR of the particles should be taken into account because of possible over-drying process of the re-hydrated particles with large surface areas compared to the commercial filler samples. Nevertheless, despite of the dried large surface, the water bound stably within the hydrogel particles should still represent main contribution to the increase of the particles' weight. The MSR of mHA/PVP and mHA/PEG is slightly lower than mHA, indicating a reduced water absorption in the presence of semi-interpenetrated network with synthetic PVP and PEG. Thus, we speculate that mHA/PVP and mHA/PEG particles may have a longer *in vivo* retention, in favour of drug delivery or filling performance which would require further tests in animal model.

3.6 *In vitro* enzymatic degradation kinetics

The Morgan-Elson reaction is a widely used method to evaluate the degradation products of HA.[44] As fragments of membrane-bound PH-20 enzymes,[45] hyaluronidases from tests have been shown to degrade HA macromolecules mainly into tetrasaccharides,[46, 47] when complete degradation takes place.

The measured concentrations of N-acetyl-D-glucosamine were 0.003 ± 0.001, 0.003 ± 0.001, 0.004 ± 0.001 mol/L at the 1.5-hour point, for mHA/PVP, mHA/PEG and mHA, respectively. At the 3-h point, the concentrations went up to 0.004 ± 0.001, 0.005 ± 0.0005, and 0.006 ± 0.003 mol/L, respectively. The functionalized particles showed a trend that they degraded slightly more slowly than mHA. Considering the molecular network within the particles, the modification of PVP/PEG had two contradictive effects on enzymatic degradation. On one hand, the incorporation of these polymers into the hydrogel network may interfere with the formation of more stable crosslinking networks among HA macromolecules, in favour of fast degradation when the HA molecules were exposed to hyaluronidases. On the other hand, the

24

modification would reduce such an exposure at the interfaces. Based on the colorimetry assay, it appeared that the two contradictive effects offset each other, and resulted in degradation kinetics similar to that of mHA. This result indicated the possibility to functionalize HA as needed without significantly changing the degradation profile.

3.7 Effects on thrombosis

Whether or not the microgels would activate the coagulation cascade reaction is clinically significant. In the clinical scenario where blood vessels are blocked by the microgel particles, those gel emboli tending to cause secondary thrombosis would complicate the embolism and worsen the local ischemia. Thromboelastography (TEG) was selected to evaluate the effects on thrombosis, as it provided essential results reflecting the comprehensive interactions in the whole blood, including:

- R value: the time until the very first evidence that a clot is detected;

- K value: the duration between R and the time when the clot grows to 20mm;

- Angle α: the tangent of the curve plotted when the K value is obtained;

- Maximum amplitude (MA): the maximum amplitude of the curve plotted, reflecting the strength of the clot.

Based on the above-mentioned four essential values, the coagulation index (CI) can be calculated with a formula provided by the manufacturer. The CI value is a simple and useful clinical index that reflect the overall status of coagulability.

$$CI = 0.3258R - 0.1886K + 0.1224MA + 0.0759\alpha - 7.7922$$

The reference range of CI is from -3.0 to +3.0. A CI value greater than +3.0 indicates a status of hypercoagulation, while a CI value less than -3.0 means hypocoagulation.

25

Table 3. Essential values obtained with thromboelastography

Group	Angle α (°)	Maximum amplitude (mm)	R (min)	K (min)	Coagulation index
mHA/PVP	32.9 ± 4.48	44.6 ± 3.04	11.83 ± 4.01	6.13 ± 1.15	2.86 ± 0.74
mHA/PEG	20.73 ± 2.51	28.67 ± 1.46	17.40 ± 1.57	10.17 ± 1.53	1.04 ± 0.12
mHA	25.93 ± 5.48	31.13 ± 0.85	16.40 ± 2.25	7.97 ± 2.45	1.83 ± 0.96
Commercial filler	30.47 ± 9.45	42.70 ± 3.70	14.37 ± 3.61	6.73 ± 2.30	3.15 ± 0.27

The essential values obtained by TEG applied to the present study in fresh citrated whole blood, listed in Table 3. The mHA/PVP seemed to have no effect on either the rate of thrombosis (p>0.999) or the strength of the clot (p=0.892). Both mHA (p< 0.001) and mHA/PEG (p<0.001) appeared able to decrease the strength of the clot, but only mHA/PEG was found to slow down the thrombosis process (p=0.048). This suggests that blood clots involving mHA/PEG may have a higher influence on thrombolysis therapy. Whether the dumbbell shape of the particles or the surface chemistry of PEG or both contributed to the low thrombosis effect of mHA/PEG merits further investigation. Based on the CI values in Table 3, the microgels prepared with our protocol were not found to influence the overall coagulability. This suggests that secondary thrombosis may serve as a minor cause after the microgels were injected into a blood vessel. Thus, in case the blood vessel is blocked in such a scenario, the gel emboli resulting from microgel aggregates can be considered as the main cause. However, as mentioned in section 3.4, no such aggregates were observed during the microfluidic experiments mimicking a surgical procedure under physiological condition. As a result, all three microgels seem to have a superior hemocompatibility, compared to the commercial filler.
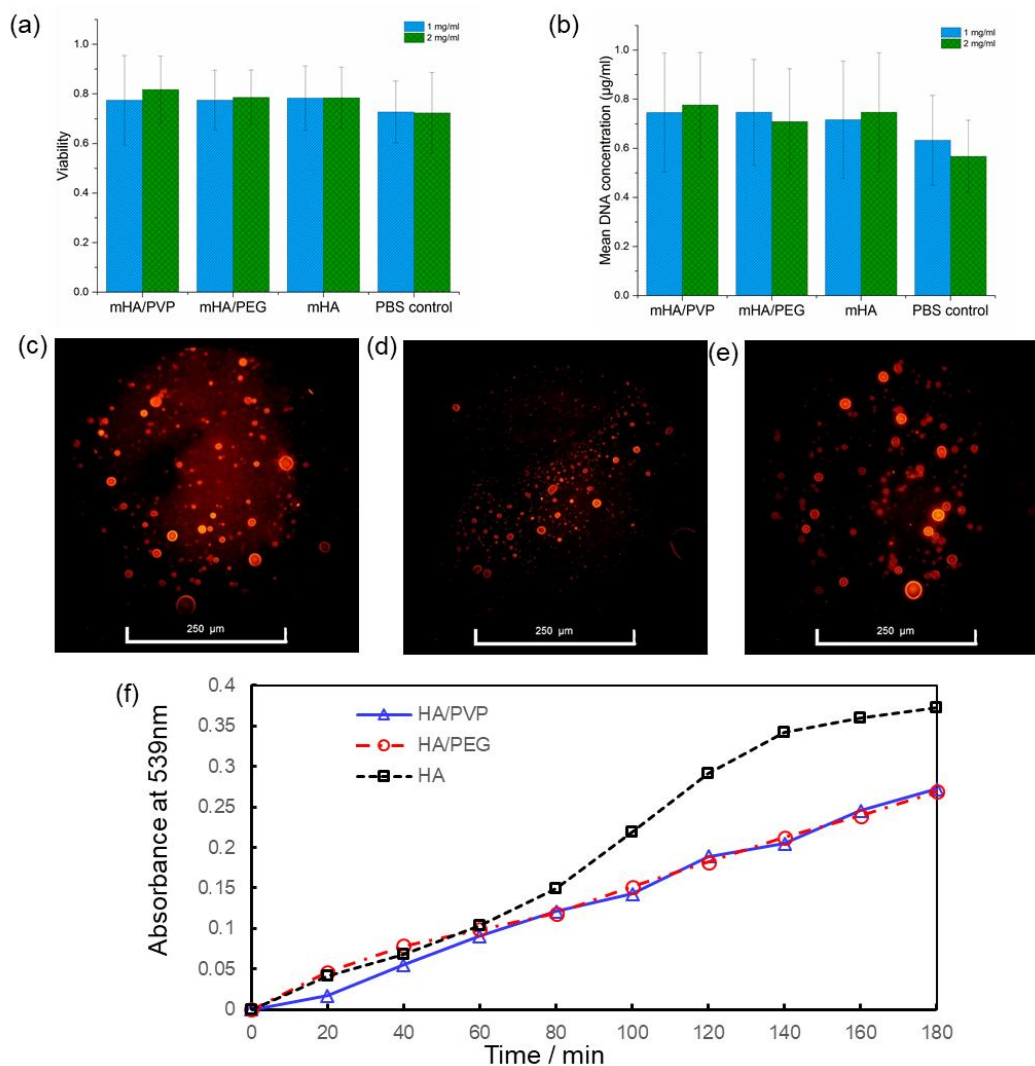
3.8 Subacute cytotoxicity

Figure 5 (a) AlamarBlue assay results on day 6 (n = 3); (b) Total DNA quantification on day 6 (n=3); (c-e) Examination of Rhodamine 6G loading status using 532 nm light. Separate dots emitting strong yellow light were observed, indicating the dye was encapsulated within hydrogel particles. (f) *In vitro* releasing kinetics of Rhodamine 6G from hydrogel particles, with enzymatic degradation, measured at 539nm.

The metabolic level and the viability of human dermal fibroblasts were evaluated with the alamarBlue assay and total DNA quantification, respectively (Fig. 5a and 5b). AlamarBlue assay has been widely used to assess cell viability and cytotoxicity via cell metabolic activity. In the alamarBlue assay, no toxic effects were observed (Fig. 5a). With both particle concentrations, the metabolic level in different groups was found to be similar to each other

27

(ANOVA; 1 mg/ml, p = 0.71; 2 mg/ml, p = 0.316). The viability was evaluated with the total DNA quantification (ANOVA; 1 mg/ml, p = 0.557; 2 mg/ml, p = 0.084) (Fig. 5b), supporting the result of the alamarBlue assay. All the experiment groups demonstrated a trend that the crosslinked particles were in favour of cell survival.

In the present study, single doses of suspensions at two different final concentrations (i.e. 1 mg/ml and 2 mg/ml) were given to cell cultures (6200 cells/well). On day 6, both the results of the alamarBlue assay and the total DNA quantification showed that the hydrogel particles had no significant negative effects on cellular metabolism or viability, compared to the PBS control. This indicates that HA-based hydrogel particles have a minimal subacute toxicity, if any. Similar results were observed in other HA hydrogel and HA-containing microparticles.[49] The results further prove that HA, as an important member of the cellular matrix, is able to enhance cell spreading, migration, and proliferation.[50] In addition, the relatively stiffer surfaces of crosslinked hydrogel particles, the uneven particle sizes, and the shapes of individual particles may increase the complexity of the local topography surrounding the cells, and thus may result in complex interactions with the cytoskeleton system.[51]

3.9 Preliminary loading and release test

To assess whether the functionalized particles were able to load hydrophilic compounds, a hydrophilic dye, Rhodamine 6G, was selected as the representative compound. The loading status of Rhodamine 6G in hydrogel particles was qualitatively examined under a fluorescent microscope, stimulated with 532 nm light. Under the microscope (×40), separate bright yellow dots were observed, which indicated that the hydrophilic dye was successfully incorporated into the particles (Fig. 5c-e).

The *in vitro* release kinetics was assessed in a hyaluronidase environment by recording the absorbance of the supernatant at 539 nm. A steady release was observed with mHA/PVP and mHA/PEG, while mHA demonstrated a burst release of the dye (Fig. 5f). As mentioned previously, the degradation kinetics was similar for all three particles. As a result, the releasing kinetics shown in Fig. 5e mainly reflected the spontaneous release. The figure showed a higher level of releasing with mHA, while the functionalized HA particles (mHA/PVP and mHA/PEG) showed a steady release rate during the 3 hours exposed to the hyaluronidase solution. This result indicated that the densely packed mHA/PVP and mHA/PEG particles and intact backbone chains of PVP and PEG may impede the loss of entrapped Rhodamine 6G. It would be important for drug delivery systems, as the result suggested the possibility that the degradation and the releasing kinetics can be modified separately.

4. Conclusion

Three kinds of HA-based hydrogel particles, mHA/PVP, mHA/PEG, and mHA, have been developed and served as the representatives of non-covalent, covalent semi-interpenetrating and conventional 3D molecular networks, respectively. Hydrogel micro-particles exhibited diameters between 2.5 and 3.5 μm and their structure and properties depended on the nature of the polymer introduced to the network. The smooth spherical mHA/PVP particles and biconcave mHA/PEG particles indicate the denser chain packing throughout the network, compared with porous irregular mHA particles. The rheological tests confirmed the tuneable, shear-thinning property of the suspensions, in addition to an improved injection controllability, compared to the commercial bulk filler. The safety profiles of the hydrogel particles were tested in terms of the dynamic dispersity and stability in microchannels, subacute cytotoxicity, and the effects on thrombosis. All particle suspensions showed superior performance

29

compared to the commercial filler. The particles also demonstrated the capacity to load and release hydrophilic compounds. Among the particles, the modified ones seemed to be superior to the unmodified HA particles, in terms of injectability, dispersity, and drug releasing kinetics. Spherical mHA/PVP particle suspensions exhibited the most desirable linear (nearly Newtonian) flow behaviour, dynamic dispersity, and stability. Based on the results above, modified HA-based particles are promising materials for new soft tissue fillers and drug delivery. Hence, the development of a micro-hydrogel system by formation of semi-interpenetrating 3D network has been demonstrated as a cost-effective way to develop novel hydrogel and hydrogel particles for meeting various medical needs.

Supporting Information

Acknowledgements

References

[1] J. Song, E. Saiz, C.R. Bertozzi, A new approach to mineralization of biocompatible hydrogel scaffolds: an efficient process toward 3-dimensional bonelike composites, J Am Chem Soc, 125 (2003) 1236-1243.
[2] T.R. Hoare, D.S. Kohane, Hydrogels in drug delivery: Progress and challenges, Polymer, 49 (2008) 1993-2007.
[3] S. Masket, J.A. Hovanesian, J. Levenson, F. Tyson, W. Flynn, M. Endl, P.A. Majmudar, S. Modi, R. Chu, M.B. Raizman, S.S. Lane, T. Kim, Hydrogel sealant versus sutures to prevent fluid egress after cataract surgery, J Cataract Refr Surg, 40 (2014) 2057-2066.
[4] J.T. Kim, D.Y. Lee, E.J. Kim, J.W. Jang, N.I. Cho, Tissue Response to Implants of Hyaluronic Acid Hydrogel Prepared by Microbeads, Tissue Engineering and Regenerative Medicine, 11 (2014) 32-38.
[5] C. DeLorenzi, Complications of Injectable Fillers, Part 2: Vascular Complications, Aesthet Surg J, 34 (2014) 584-600.
[6] J. Cohen, O. Onwudiwe, Vascular Compromise After Hyaluronic Acid Cheek Augmentation, Journal of Drugs in Dermatology, 11 (2012) S12-S14.
[7] X.F. Han, J.T. Hu, L. Cheng, F.C. Li, Multiplane hyaluronic acid (EME) in female Chinese rhinoplasty using blunt and sharp needle technique, Journal of Plastic Reconstructive and Aesthetic Surgery, 68 (2015) 1504-1509.
[8] W. Wu, I. Carlisle, P. Huang, N. Ribe, R. Russo, C. Schaar, A. Verpaele, A. Strand, Novel Administration Technique for Large-Particle Stabilized Hyaluronic Acid-Based Gel of Nonanimal Origin in Facial Tissue Augmentation, Aesthetic Plastic Surgery, 34 (2010) 88-95.

[9] K. Ajisaka, Y. Iwashita, MODIFICATION OF HUMAN-HEMOGLOBIN WITH POLYETHYLENE-GLYCOL - A NEW CANDIDATE FOR BLOOD SUBSTITUTE, Biochemical and Biophysical Research Communications, 97 (1980) 1076-1081.

[10] K. Taguchi, Y. Urata, M. Anraku, H. Watanabe, D. Kadowaki, H. Sakai, H. Horinouchi, K. Kobayashi, E. Tsuchida, T. Maruyama, M. Otagiri, Hemoglobin Vesicles, Polyethylene Glycol (PEG)ylated Liposomes Developed as a Red Blood Cell Substitute, Do Not Induce the Accelerated Blood Clearance Phenomenon in Mice, Drug Metabolism and Disposition, 37 (2009) 2197-2203.

[11] B. Butruk, M. Trzaskowski, T. Ciach, Polyvinylpyrrolidone-Based Coatings for Polyurethanes - the Effect of Reagent Concentration on Their Chosen Physical Properties, Chem Process Eng-Inz, 33 (2012) 563-571.

[12] F.W. Hartman, V.G. Behrmann, The Present Status of Plasma Expanders, Jama-J Am Med Assoc, 152 (1953) 1116-1120.

[13] C. Mao, Y.Z. Qiu, H.B. Sang, H. Mei, A.P. Zhu, J. Shen, S.C. Lin, Various approaches to modify biomaterial surfaces for improving hemocompatibility, Adv Colloid Interfac, 110 (2004) 5-17.

[14] H.J. Cho, I.S. Yoon, H.Y. Yoon, H. Koo, Y.J. Jin, S.H. Ko, J.S. Shim, K. Kim, I.C. Kwon, D.D. Kim, Polyethylene glycol-conjugated hyaluronic acid-ceramide self-assembled nanoparticles for targeted delivery of doxorubicin, Biomaterials, 33 (2012) 1190-1200.

[15] N. Sahiner, W. Godbey, G.L. McPherson, V.T. John, Microgel, nanogel and hydrogel–hydrogel semi-IPN composites for biomedical applications: synthesis and characterization, Colloid and Polymer Science, 284 (2006) 1121-1129.

[16] A. Schwarz, H. Zhang, A. Metcalfe, I. Salazkin, J. Raymond, Transcatheter embolization using degradable crosslinked hydrogels, Biomaterials, 25 (2004) 5209-5215.

[17] S. Mueller, E.W. Llewellin, H.M. Mader, The rheology of suspensions of solid particles, Proceedings of the Royal Society a-Mathematical Physical and Engineering Sciences, 466 (2010) 1201-1228.

[18] J.M. Sherwood, E. Kaliviotis, J. Dusting, S. Balabani, Hematocrit, viscosity and velocity distributions of aggregating and non-aggregating blood in a bifurcating microchannel, Biomechanics and modeling in mechanobiology, 13 (2014) 259-273.

[19] D.C. Duffy, J.C. McDonald, O.J. Schueller, G.M. Whitesides, Rapid Prototyping of Microfluidic Systems in Poly(dimethylsiloxane), Analytical chemistry, 70 (1998) 4974-4984.

[20] E. Esposito, E. Menegatti, R. Cortesi, Hyaluronan-based microspheres as tools for drug delivery: a comparative study, Int J Pharm, 288 (2005) 35-49.

[21] O. Shamsara, Z.K. Muhidinov, S.M. Jafari, J. Bobokalonov, A. Jonmurodov, M. Taghvaei, M. Kumpugdee-Vollrath, Effect of ultrasonication, pH and heating on stability of apricot gum-lactoglobuline two layer nanoemulsions, International journal of biological macromolecules, 81 (2015) 1019-1025.

[22] X. Jia, Y. Yeo, R.J. Clifton, T. Jiao, D.S. Kohane, J.B. Kobler, S.M. Zeitels, R. Langer, Hyaluronic acid-based microgels and microgel networks for vocal fold regeneration, Biomacromolecules, 7 (2006) 3336-3344.

[23] D.K. Chhetri, A.H. Mendelsohn, Hyaluronic acid for the treatment of vocal fold scars, Curr Opin Otolaryngo, 18 (2010) 498-502.

[24] M.N. Collins, C. Birkinshaw, Comparison of the effectiveness of four different crosslinking agents with hyaluronic acid hydrogel films for tisslue-culture applications, Journal of Applied Polymer Science, 104 (2007) 3183-3191.

[25] M.N. Collins, C. Birkinshaw, Investigation of the swelling behavior of crosslinked hyaluronic acid films and hydrogels produced using homogeneous reactions, Journal of Applied Polymer Science, 109 (2008) 923-931.

[26] A.A.M. Shimojo, A.M.B. Pires, R. Lichy, A.A. Rodrigues, M.H.A. Santana, The crosslinking degree controls the mechanical, rheological, and swelling properties of

31

hyaluronic acid microparticles, Journal of Biomedical Materials Research Part A, 103 (2015) 730-737.

[27] H.J. Deuling, W. Helfrich, Red Blood-Cell Shapes as Explained on Basis of Curvature Elasticity, Biophys J, 16 (1976) 861-868.

[28] L. Rieppo, S. Saarakkala, T. Narhi, H.J. Helminen, J.S. Jurvelin, J. Rieppo, Application of second derivative spectroscopy for increasing molecular specificity of fourier transform infrared spectroscopic imaging of articular cartilage, Osteoarthr Cartilage, 20 (2012) 451-459.

[29] H.J. Mcdonald, R.H. Spitzer, Polyvinylpyrrolidone - the Electromigration Characteristics of the Blood Plasma Expander, Circ Res, 1 (1953) 396-404.

[30] K.A. Huynh, K.L. Chen, Aggregation Kinetics of Citrate and Polyvinylpyrrolidone Coated Silver Nanoparticles in Monovalent and Divalent Electrolyte Solutions, Environ Sci Technol, 45 (2011) 5564-5571.

[31] V.I. Teberekidis, M.P. Sigalas, Theoretical study of hydrogen bond interactions of felodipine with polyvinylpyrrolidone and polyethyleneglycol, J Mol Struc-Theochem, 803 (2007) 29-38.

[32] R. Duelli, W. Kuschinsky, Changes in Brain Capillary Diameter during Hypocapnia and Hypercapnia, J Cerebr Blood F Met, 13 (1993) 1025-1028.

[33] S.W. Park, S.J. Woo, K.H. Park, J.W. Huh, C. Jung, O.K. Kwon, Iatrogenic Retinal Artery Occlusion Caused by Cosmetic Facial Filler Injections, Am J Ophthalmol, 154 (2012) 653-662.

[34] M.S. Dwyer, L.J. Melton, D.J. Ballard, P.J. Palumbo, J.C. Trautmann, C.P. Chu, Incidence of Diabetic-Retinopathy and Blindness - a Population-Based Study in Rochester, Minnesota, Diabetes Care, 8 (1985) 316-322.

[35] M. Iwanaga, K. Kamoi, Patient Perceptions of Injection Pain and Anxiety: A Comparison of NovoFine 32-Gauge Tip 6mm and Micro Fine Plus 31-Gauge 5mm Needles, Diabetes Technol The, 11 (2009) 81-86.

[36] J.B. Segur, H.E. Oberstar, Viscosity of Glycerol and Its Aqueous Solutions, Ind Eng Chem, 43 (1951) 2117-2120.

[37] R.S. Rosenson, A. McCormick, E.F. Uretz, Distribution of blood viscosity values and biochemical correlates in healthy adults, Clin Chem, 42 (1996) 1189-1195.

[38] J.K. Nunes, S.S. Tsai, J. Wan, H.A. Stone, Dripping and jetting in microfluidic multiphase flows applied to particle and fiber synthesis, J Phys D Appl Phys, 46 (2013) 114002.

[39] A. Kumar, R.G.H. Rivera, M.D. Graham, Flow-induced segregation in confined multicomponent suspensions: effects of particle size and rigidity, Journal of Fluid Mechanics, 738 (2014) 423-462.

[40] K.A. Kusters, J.G. Wijers, D. Thoenes, Aggregation kinetics of small particles in agitated vessels, Chem Eng Sci, 52 (1997) 107-121.

[41] E. Kaliviotis, J.M. Sherwood, S. Balabani, Partitioning of red blood cell aggregates in bifurcating microscale flows, Sci Rep, 7 (2017) 44563.

[42] S.A. Bencherif, A. Srinivasan, F. Horkay, J.O. Hollinger, K. Matyjaszewski, N.R. Washburn, Influence of the degree of methacrylation on hyaluronic acid hydrogels properties, Biomaterials, 29 (2008) 1739-1749.

[43] J.B. Leach, K.A. Bivens, C.W. Patrick, C.E. Schmidt, Photocrosslinked hyaluronic acid hydrogels: Natural, biodegradable tissue engineering scaffolds, Biotechnology and Bioengineering, 82 (2003) 578-589.

[44] E.S.A. Hofinger, J. Hoechstetter, M. Oettl, G. Bernhardt, A. Buschauer, Isoenzyme-specific differences in the degradation of hyaluronic acid by mammalian-type hyaluronidases, Glycoconjugate J, 25 (2008) 101-109.

[45] M.F. Meyer, G. Kreil, H. Aschauer, The soluble hyaluronidase from bull testes is a fragment of the membrane-bound PH-20 enzyme, Febs Lett, 413 (1997) 385-388.

[46] K. Sugahara, Y. Tanaka, S. Yamada, Preparation of a series of sulfated tetrasaccharides from shark cartilage chondroitin sulfate D using testicular hyaluronidase and structure determination by 500 MHz H-1 NMR spectroscopy, Glycoconjugate J, 13 (1996) 609-619.

[47] J.A. Cramer, L.C. Bailey, C.A. Bailey, R.T. Miller, Kinetic and Mechanistic Studies with Bovine Testicular Hyaluronidase, Bba-Gen Subjects, 1200 (1994) 315-321.

[48] K.R. Machlus, J.C. Cardenas, F.C. Church, A.S. Wolberg, Causal relationship between hyperfibrinogenemia, thrombosis, and resistance to thrombolysis in mice, Blood, 117 (2011) 4953-4963.

[49] I. Eroglu, E.H. Gokce, N. Tsapis, S.T. Tanriverdi, G. Gokce, E. Fattal, O. Ozer, Evaluation of characteristics and in vitro antioxidant properties of RSV loaded hyaluronic acid-DPPC microparticles as a wound healing system, Colloid Surface B, 126 (2015) 50-57.

[50] B. Duan, L.A. Hockaday, E. Kapetanovic, K.H. Kang, J.T. Butcher, Stiffness and adhesivity control aortic valve interstitial cell behavior within hyaluronic acid based hydrogels, Acta Biomaterialia, 9 (2013) 7640-7650.

[51] Z. Wang, G. Wu, S. Bai, Z. Feng, Y. Dong, J. Zhou, H. Qin, Y. Zhao, MAPs/bFGF-PLGA microsphere composite-coated titanium surfaces promote increased adhesion and proliferation of fibroblasts, Biomed Mater, 9 (2014) 035006.

33

Figure Captions:

Figure 1. (a)-(c) Schematic showing semi-interpenetrating network of HA/PVP (a). interpenetrating network of HA/PEG (b) and network of HA(c). (d) FTIR spectra of the three hydrogel microparticles. (e) Vector normalized second order derivative FTIR spectra between 1575 and 1595 cm^{-1}, generated with the Savitsky-Golay algorithm, which narrowed the bandwidths and increased the resolution of differential spectra. In uncrosslinked hyaluronic acid, the peak around 1585 cm-1 represented N-H bending, which was used as a marker of HA molecules.

Figure 2. SEM images showing the morphology of microparticles made from mHA/PVP (a) and (d), mHA/PEG (b) and (e) and mHA (c) and (f).

Figure 3. (a) Shear stress versus shear rate curves of particle suspensions and the commercial filler, and fitting with the Herschel-Bulkley model. (b) Effective viscosity versus shear rates curves of particle suspensions and the commercial filler. (c) Frequency dependence of storage modulus G' and lost modules G'' of the three suspensions. (d) Frequency dependence of storage modulus G' and lost modules G'' of the commercial filler.

Figure 4. a) Schematic of A T-junction microfluidic system. (b-j) The flow fields of three particle suspensions at the T-injection port (b, e, h) and the site 1 cm away (c, f, i). As the arrow indicates, a 35% glycerol solution was fed into the main channel using a syringe pump. (d), (g) and (j) show the velocity distribution of three particle suspensions (external injection pressure = 28 kPa). The velocity vectors are normalised with the average velocity across the microfluidic channel obtained from the combined flowrate of the two streams in order to

facilitate comparisons. The red indicates high velocity, while blue low velocity. (b, c, d) mHA/PVP; (e, f, g) mHA/PEG; (h, i, j) mHA.

Figure 5 (a) AlamarBlue assay results on day 6 (n = 3); (b) Total DNA quantification on day 6 (n=3); (c-e) Examination of Rhodamine 6G loading status using 532 nm light. Separate dots emitting strong yellow light were observed, indicating the dye was encapsulated within hydrogel particles. (f) *In vitro* releasing kinetics of Rhodamine 6G from hydrogel particles, with enzymatic degradation, measured at 539nm.

Tables:

Table 1. Summary of structure and properties of the peaks detected in hydrogel particle suspensions

	mHA/PVP	mHA/PEG	mHA
DLS No. of peak	1	1	1
Particle diameter/ μm	2.80 ± 0.35	3.70 ± 0.38	2.74 ± 0.310
Polydispersity index, PDI	0.07 ± 0.03	0.08 ± 0.03	0.08 ± 0.02
Relative HA content%	56	80	83.6
Mass swelling ratio, MSR	7.01	7.93	10.40

Table 2. Rheological parameters of three hydrogel particle suspensions from Herschel-Bulkley model.

	HA/PVP	HA	HA/PEG
Yield stress, τ_y	0	0	0
$\sigma (\tau_y)$	0.58	5.82	9.32
Consistency, K	2.31	26.66	41.93
$\sigma (K)$	0.16	3.71	6.28
Flow index, n	0.8	0.46	0.44
$\sigma (n)$	0.01	0.03	0.03

Table 3. Essential values obtained with thromboelastography

Group	Angle α (°)	Maximum amplitude (mm)	R (min)	K (min)	Coagulation index
mHA/PVP	32.9 ± 4.48	44.6 ± 3.04	11.83 ± 4.01	6.13 ± 1.15	2.86 ± 0.74
mHA/PEG	20.73 ± 2.51	28.67 ± 1.46	17.40 ± 1.57	10.17 ± 1.53	1.04 ± 0.12
mHA	25.93 ± 5.48	31.13 ± 0.85	16.40 ± 2.25	7.97 ± 2.45	1.83 ± 0.96
Commercial filler	30.47 ± 9.45	42.70 ± 3.70	14.37 ± 3.61	6.73 ± 2.30	3.15 ± 0.27

Graphical abstract